CROATICA CHEMICA ACTA CCACAA **70** (2) 719–734 (1997)

ISSN–0011-1643
CCA–2448 *Original Scientific Paper*

Formation and Characterization of $NiFe_2O_4$

Svetozar Musić,[a] *Davor Balzar,*[a] *Stanko Popović,*[a,b] *Marijan Gotić,*[a] *Ilona Czakó-Nagy,*[c] *and Samet Dalipi*[a]

[a]*Ruđer Bošković Institute, P. O. Box 1016, 10001 Zagreb, Croatia*

[b]*Department of Physics, Faculty of Science, University of Zagreb, P. O. Box 162, 10001 Zagreb, Croatia*

[c]*Department of Nuclear Chemistry, Eötvös Loránd University, P. O. Box 32, 1518 Budapest, Hungary*

Received January 25, 1996; revised June 4, 1996; accepted June 7, 1996

Synthesis of nickel ferrite, $NiFe_2O_4$, was performed applying the thermal treatment of the corresponding mixed metal hydroxides or the solid state reaction between NiO and α-Fe_2O_3. The samples were studied by X-ray diffraction, Fourier transform IR spectroscopy and ^{57}Fe Mössbauer spectroscopy. Ball-milling of $NiFe_2O_4$ caused a decrease of hyperfine magnetic fields corresponding to Fe^{3+} ions in tetrahedral and octahedral sites, an increase of the Mössbauer spectral line widths, as well as a slight increase of isomer shifts. It was supposed that the ball-milling of $NiFe_2O_4$ had more influence on the degree of inversion than on other structural properties of the spinel. It was found that the heating temperature, and not the heating time, had the ultimate effect on $NiFe_2O_4$ microstructure. Samples heated up to 500 °C showed a pronounced size-correlated diffraction line broadening, corresponding to the coherent domain size of about 13 nm, and rather small crystalline disorder. Samples heated at temperatures above ≈ 1000 °C had much larger crystallites, exhibiting very small disorder.

INTRODUCTION

Nickel ferrite is an inverse spinel in which the tetrahedral or A-sites are occupied by Fe^{3+} ion, and the octahedral or B-sites by Fe^{3+} and Ni^{2+} ions. Fully inverse nickel ferrite is described by the structural formula $(Fe^{3+})_A[Ni^{2+}Fe^{3+}]_BO_4^{2-}$. Nickel ferrite and substituted nickel ferrites are the materials of interest for the application in electronic technology. These materials, besides specific magnetic properties, are characterized by a strong absorption of electromagnetic radiation in the microwave frequency range and, due to these properties, they have a potential use in devices for telecommunication measurements, or as surface coatings on aircraft or missle structures.[1] Nickel ferrites of different stoichiometry are also found in the rust formed by corrosion of nickel containing alloys.

Scientists and engineers have investigated nickel ferrite, as well as substituted nickel ferrites from different standpoints. For instance, Morrish and Haneda[2] prepared $NiFe_2O_4$ particles of average sizes 250 ± 50, 800 ± 200 and 1300 ± 200 Å. The authors suggested a non-collinear magnetic structure near the surface of $NiFe_2O_4$ particles. In accordance with this suggestion, small $NiFe_2O_4$ particles consisted of a core with the usual spin arrangement and a surface layer with magnetic moments inclined to the direction of the net magnetization. A non-collinear magnetic structures near the surface of γ-Fe_2O_3, ^{57}Fe surface-enriched γ-Fe_2O_3, ^{57}Fe-doped CrO_2 and α-Fe particles were also observed.[3]

Mixed hydroxides $Ni(OH)_2/Fe(OH)_3$, containing up to $x = 0.10$ NiO, were thermally treated in order to prepare $NiFe_2O_4$.[4] NiO was found to be soluble in α-Fe_2O_3 at 550 °C ($x_{NiO} = 2\%$), and the formation of $NiFe_2O_4$ was also observed for a bigger content of NiO. When the stoichiometric ratio for $NiFe_2O_4$ formation was used, the precursor of $NiFe_2O_4$ was observed at ≈ 185 °C, which was transformed to amorphous ferrite at ≈ 275 °C and to crystalline $NiFe_2O_4$ above 400 °C. Morozumi *et al.*[5] hydrothermally treated the mixed hydroxides, $Ni(OH)_2/Fe(OH)_3$, up to 250 °C. Formation of nickel ferrite precursor was observed at 75 °C, and of nickel ferrite at temperatures above 100 °C.

Mixed hydroxides, $Ni(OH)_2/Fe(OH)_3$, containing different molar fractions of NiO and Fe_2O_3, were thermally treated up to 800 or 1100 °C.[6] Oxide phases α-Fe_2O_3, NiO and $NiFe_2O_4$ were detected in the samples prepared at 800 °C. The samples prepared at 1100 °C contained one more phase, with the structure similar to stoichiometric $NiFe_2O_4$. Formation of oxide phases, generated during the synthesis of $NiFe_2O_4$ by thermal decomposition of the mixed salts, $Ni(NO_3)_2/Fe(NO_3)_3 \cdot nH_2O$, NiO : Fe_2O_3 = 1 : 1, was also investigated.[7] Peev *et al.*[8] examined the thermal decomposition of the salt $Ni_{0.33}Fe_{0.67}(NH_4)_2(SO_4)_2 \cdot 6H_2O$ using thermal analysis and Mössbauer spectroscopy. The optimum temperature for $NiFe_2O_4$ formation was found to be 900 °C.

Mössbauer spectra of several samples, prepared in the system $Ni_xFe_{3-x}O_4$, $0 \leq x \leq 1$, were recorded at room temperature.[9] The rapid electron exchange between Fe^{2+} and Fe^{3+} ions in the same lattice site was shown. MacKenzie and Cardile[10] investigated the formation of nickel ferrite from NiO and spinel iron-sand found on the west coast of New Zealand's North Island.

Spherical and hollow $NiFe_2O_4$ particles were produced using the method of aerosol pyrolysis.[11] Aerosol droplets, containing a dilute aqueous solution of $Ni(NO_3)_2$ + $Fe(NO_3)_3$ with stoichiometric ratio for $NiFe_2O_4$ formation, were thermally treated between 450 and 810 °C.

The principal corrosion product, formed in the stainless steel primary cooling circuit of a PWR (Pressurized Water Reactor), is generally accepted to be a nonstoichiometric nickel ferrite, $Ni_xFe_{3-x}O_4$, $0.45 < x < 0.75$.[12] Raw[13] investigated variously prepared samples of magnetite and nickel ferrite in simulation of corrosion products. The Ni-substituted magnetite ($x \approx 0.5$) and $NiFe_2O_4$ were detected in the rust formed by the heating of Fe-Ni alloys in air at 635 °C.[14] Lenglet *et al.*[15] characterized the oxidation products formed on stainless steel (18Cr-10Ni-2Mn) at 900–1100 °C using the X-ray diffraction, conversion electron Mössbauer spectroscopy and Fourier transform spectroscopy. Cr_2O_3, $MnCr_2O_4$ and α-Fe_2O_3 were detected as oxidation products on the steel surface, but not $NiFe_2O_4$, NiO and $NiCr_2O_4$.

The aim of the present work was to obtain more information about the chemical and structural properties of $NiFe_2O_4$ formed under different experimental conditions. Special attention was paid to the influence of mechanical treatment on the structural properties of $NiFe_2O_4$.

EXPERIMENTAL

All chemicals were of *p.a.* purity. Two methods of the $NiFe_2O_4$ preparation were used. Samples S_1 to S_6 were prepared using mixed hydroxides obtained from the $Ni(NO_3)_2$ + $Fe(NO_3)_3$ solution by addition of the NaOH solution. The mixed hydroxides $Ni(OH)_2/Fe(OH)_3$, NiO : Fe_2O_3 = 1 : 1, were washed from »neutral« electrolyte and then heated at different temperatures, as given in Table I. A LKO II furnace with Kanthal heaters was used at temperatures above 1000 °C. Samples S_7 to S_{11} were prepared using the solid state reaction between NiO and α-Fe_2O_3 in stoichiometric ratio for the $NiFe_2O_4$ formation. The mixture of NiO and α-Fe_2O_3 , used for the preparation of samples S_7 and S_8, was mechanically activated for 15 to 60 minutes, respectively, while the time of mechanical activation in the preparation of samples S_9, S_{10} or S_{11} was 3 hours. A planetary mill by Fritsch (pulverisette 5, agate bowl with balls of 99.9% SiO_2) was used. Mechanically treated oxide powders were pressed into tablets using a Carver press, and then heated at high temperatures, as given in Table I.

All samples were studied using the X-ray powder diffraction (XRD), Fourier transform infrared (FT-IR) spectroscopy and ^{57}Fe Mössbauer spectroscopy. XRD measurements were performed at room temperature (RT) using a Philips counter

TABLE I

Thermal treatment of the samples and their phase composition, as determined by X-ray diffraction

Sample	Heating temp. / °C	Heating time / h	Phase composition	Remarks
S_1	200	1	$NiFe_2O_4$	Sharp diffraction lines
	300	1		
	400	1		
	800	1		
	1100	1		
	1200	1		
	1350	3		
S_2	500	2	$NiFe_2O_4$ + α-Fe_2O_3 (few %)	Broad diffraction lines All samples show practically equal diffraction patterns
S_3	500	4	$NiFe_2O_4$ + α-Fe_2O_3 (few %)	
S_4	500	8	$NiFe_2O_4$ + α-Fe_2O_3 (few %)	
S_5	500	24	$NiFe_2O_4$ + α-Fe_2O_3 (few %)	
S_6	500	48	$NiFe_2O_4$ + α-Fe_2O_3 (few %)	
S_7	200	1	$NiFe_2O_4$	Very little broadened diffraction lines in comparison to S_1
	300	1		
	400	1		
	800			
	1100	1		
	1200	1		
	1350	3		
S_8	200	1	$NiFe_2O_4$	
	300	1		
	400	1		
	800	1		
	1100	1		
	1200	1		
	1350	3		
S_9	200	1	α-Fe_2O_3 + NiO	NiO-broadened diffraction lines Similar diffraction patterns
	300	1		
S_{10}	200	1	α-Fe_2O_3 + NiO	
	300	1		
	400	1		
S_{11}	200	1	$NiFe_2O_4$ + α-Fe_2O_3 (~5 %)	Very little broadened diffraction lines
	300	1		
	400	1		
	800	5		

diffractometer, model MPD 1880, with monochromatized Cu-Kα radiation (graphite monochromator). FT-IR spectra (RT) were recorded using a Perkin-Elmer spectrometer, model 2000. The FT-IR spectrometer was coupled to a personal computer loaded with the IR Data Manager (IRDM) program. Specimens for FT-IR measurements were prepared by pressing the samples with spectroscopically pure KBr or polyeth-

ylene in small pellets. Mössbauer spectra (RT) were recorded on a spectrometer produced by WISSEL. The spectra were fitted using the SIRIUS program.[16]

RESULTS AND DISCUSSION

Phase composition of the studied samples, as determined by XRD, is given in Table I.

$NiFe_2O_4$ as a single phase was obtained after heating the mixed hydroxides, $Ni(OH)_2/Fe(OH)_3$, NiO : Fe_2O_3 = 1 : 1, up to 1100 or 1350 °C, and the corresponding X-ray diffraction patterns contained sharp diffraction lines. At 500 °C, for the heating time from 2 to 48 hours, $NiFe_2O_4$ was formed as the dominant phase, exhibiting a pronounced diffraction broadening. These samples also contained a small amount of α-Fe_2O_3. It was reported that nickel ferrite could be also obtained from mixed hydroxides, $Ni(OH)_2/Fe(OH)_3$, at temperatures below 500 °C;[4,5] however, in that case, its stoichiometry and crystallinity varied significantly, and generally other oxide phases were present in the samples.

Lattice constant of $NiFe_2O_4$ (space group $Fd3m$) was determined in the present work using α-Al_2O_3 (corundum by Merck, 99.999%) as internal standard (space group $R3c$, lattice constants, in terms of hexagonal axes, a = 0.4758, c = 1.2991 nm at 26 °C, ICDD Powder Diffraction File (card no. 10–173). For sample S_1, utilizing diffraction lines at the highest possible Bragg angles, well resolved in spectral doublet components $K\alpha_1\alpha_2$ (Figure 1), a value of a = 0.83377(3) nm was obtained at 26 °C. For samples S_2 to S_6, having broad diffraction lines, not resolved in spectral components (Figure 2), practically the same value was obtained, a = 0.8338(1) nm.

Samples S_7 to S_{11}, prepared by the solid state reaction between NiO + α-Fe_2O_3 had also practically the same lattice constant as the ones obtained by precipitation from hydroxides. Samples S_7, S_8 and S_{11}, heated to high temperature, showed very little broadened diffraction lines of $NiFe_2O_4$ in comparison with sample S_1. However, samples S_9 and S_{10}, heated up to 300 and 400 °C, respectively, contained α-Fe_2O_3 and NiO, which showed broad diffraction lines.

Samples S_2 to S_6 showed a pronounced diffraction-line broadening, as compared to all the other samples heated at a much higher temperature. According to the accepted theories,[17,18] both »size« and »strain« effects cause diffraction-line broadening. The size term does not necessarily correspond to the size of particles or grains, but to the size of domains distinctly defined by incoherent diffraction, which can be caused by stacking (deformation) or twin (growth) faults, small-angle boundaries due to dislocation ordering, or similar extended lattice defects. That is why the domain size, determined by diffraction methods, is usually underestimated in relation to a size ob-

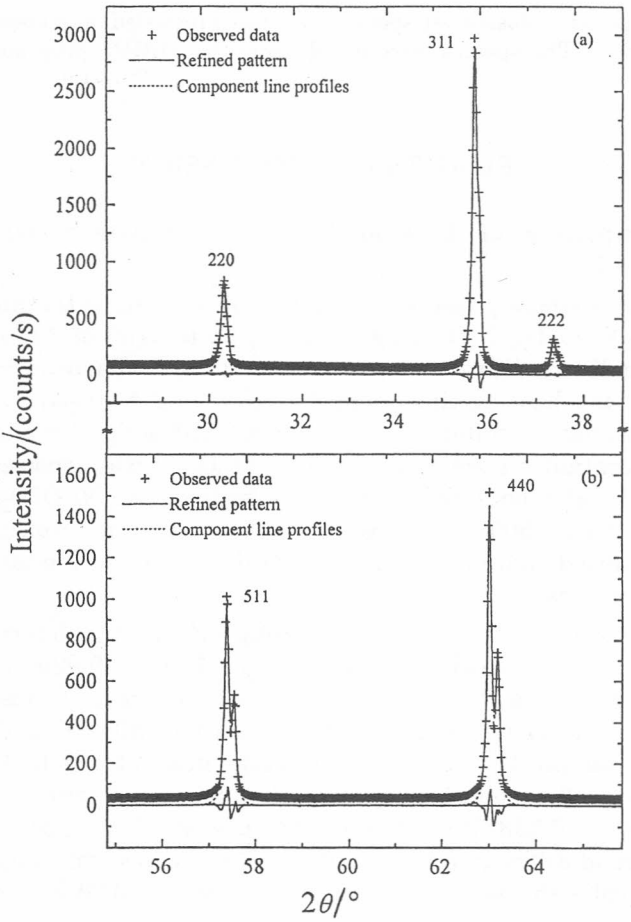

Figure 1. X-ray diffraction pattern of sample S_1. Refined pattern was obtained through the profile-fitting least-squares minimization procedure described in the text. Difference between the observed and refined patterns is plotted around the zero-intensity line. The Miller indices of diffraction lines of $NiFe_2O_4$ are denoted. Note sharp diffraction lines, which make 311 and 222 completely resolved.

tained by other, mostly optical methods (microscope, laser size analyzer, *etc.*). The strain term includes contribution from any disruption of a regular lattice, such as dislocations and point defects. Therefore, there may be at least two reasons for substantial line broadening of samples S_2 to S_6, small domain size and/or disorder at crystallographic sites, which is possible in the spinel structure. However, the fact that diffraction patterns of samples S_2 to S_6 and particularly the full width at half maximum (FWHM) of their diffraction lines did not change noticeably, regardless of heating time (see Ta-

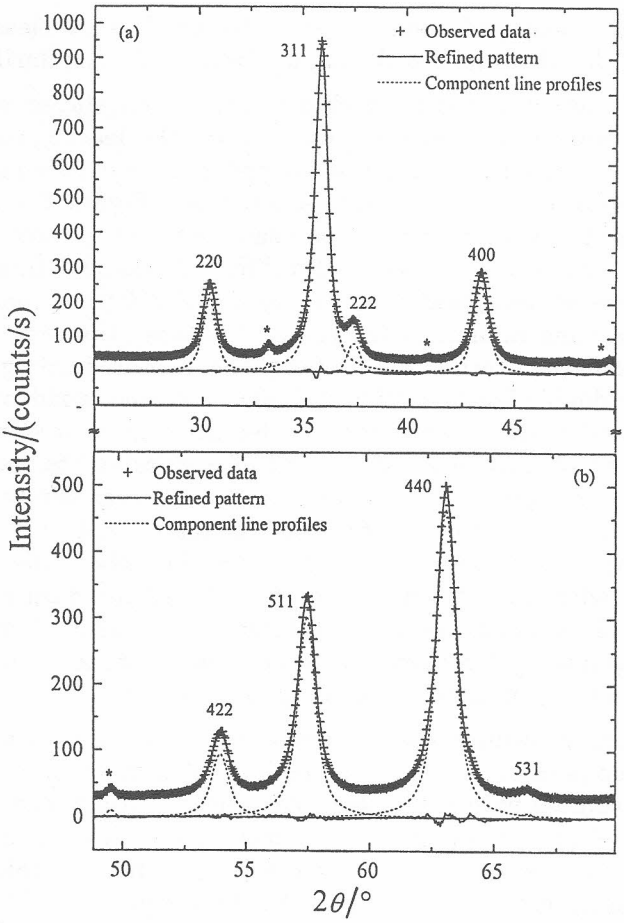

Figure 2. X-ray diffraction patterns of sample S_3. Refined pattern was obtained through the profile-fitting least-squares minimization procedure described in the text. Difference between the observed and refined patterns is plotted around the zero-intensity line. The Miller indices of diffraction lines of $NiFe_2O_4$ are denoted. Stars indicate positions of diffraction lines of a small amount of α-Fe_2O_3 impurity. Note broad diffraction lines, where 222 is partially hidden under the much stronger 311 line.

ble I), favours the former assumption. A rough estimate from FWHM using the Scherrer equation[19]

$$\langle D \rangle_v = \frac{\lambda}{\beta(2\theta)\cos\theta_0} \tag{1}$$

(λ is the X-ray wavelength, θ is a diffraction and θ_0 the Bragg angle, and the integral breadth $\beta(2\theta)$ was approximated with FWHM yields an average

coherent volume-weighted domain size of 13 nm. Nevertheless, we undertook the more detailed line-broadening analysis to further clarify this point.

It is widely accepted that the Stokes Fourier deconvolution method,[20] followed by the Warren-Averbach analysis,[18] gives the least biased approach. However, in cases of substantial line overlapping, the Stokes method generally fails due to unresolved tails of diffraction lines. Figure 2 shows characteristic parts of the diffraction pattern of sample S_3, where large overlapping of almost all lines is visible. We used a different profile-fitting approach,[21] which uses pre-set analytical functions to model different contributions to line broadening and minimizes the residual between the computed and observed diffraction patterns. The subsequent line-broadening analysis is based on the »double-Voigt« method.[22] Before any line-broadening analysis, the instrumental contribution to the broadening must be accounted for. This is accomplished by careful measurement of a suitable standard specimen showing a minimal physical (structural, specimen) broadening. Sometimes, the adequate standard can be the same material that was properly annealed. Figure 1 shows quite sharp diffraction lines of sample S_1. However, a comparison with the diffraction pattern of NIST standard reference material 660 LaB_6 showed, though not large, some residual broadening of $NiFe_2O_4$ in sample S_1. Moreover, we chose to use LaB_6 as a standard, to be able to compare the parameters of samples S_1 and S_3.

In the fitting procedure, the instrumental line profile is synthesized from pre-determined parameters which define instrumental broadening. This line profile is convoluted with a pre-set Voigt function which models the physically broadened line profile. After the background is added, the thus calculated pattern is compared to the observed data. The refinable parameters of the Voigt function are adjusted until the least-squares residual reaches a minimum. All the refined parameters of the physically broadened line profiles for seven strongest $NiFe_2O_4$ reflections for both S_1 and S_3 samples are presented in Table II. Standard uncertainties and particularly the pattern-discrepancy factors indicate somewhat larger relative errors for sample S_1, as a consequence of a similar broadening of S_1 and LaB_6 diffraction lines. Figure 3 presents the so-called Williamson-Hall plot[23] for sample S_3. The integral breadths, $\beta(s) = \beta(2\theta)\cos\theta_o/\lambda$, are plotted as a function of the variable in reciprocal space, $s = 2\sin\theta/\lambda$. It is evident that the integral breadth of 222 diffraction line is underestimated due to its overlap with the much stronger 311 line (Figure 2). We excluded that particular line from all the subsequent calculations for sample S_3 , whereas all the lines for sample S_1 were used. All other integral breadths approximately fall on the straight line, which means that broadening is isotropic. This dismisses a possible existence of growth faults in grains because it would cause an [*hkl*]-dependent broadening and line shifts, which were not observed either, in FCC spinel structure.[18] Approximately horizontal straight line indicates small strain. More detailed

TABLE II

Parameters of the Voigt function, which models the physically broadened line profile, as refined in the profile fitting for samples S_1 and S_3: Cauchy (Lorentz), β_C, and Gauss, β_G, integral breadths. The corresponding full width at half maximum (FWHM) is calculated from the Voigt integral breadth, β. Weighted pattern-discrepancy (residual) factor, $R_{wp} = 100[\Sigma w_i(I_i - I_{ci})^2/\Sigma w_i I_i^2]^{1/2}$, where w_i are weights of the observed intensities, I_i, and I_{ci} are calculated intensities

Sample	*hkl*	β_C / °	β_G / °	β / °	FWHM / °	R_{wp} / %
S_1	220	0.019(4)*	0.036(9)	0.049	0.041	5.19
	311	0.009(1)	0.019(4)	0.025	0.021	5.19
	222	$< 10^{-5}$	0.048(27)	0.048	0.045	5.19
	400	0.014	0.019(5)	0.029	0.023	4.30
	422	0.036(3)	$< 10^{-5}$	0.036	0.023	5.73
	511	0.044(2)	$< 10^{-5}$	0.044	0.028	7.81
	440	0.033(1)	$< 10^{-5}$	0.033	0.021	7.81
S_3	220	0.663(26)	0.485(24)	0.982	0.726	3.62
	311	0.836(11)	0.335(14)	0.997	0.681	3.62
	222	0.001(2)	0.725(18)	0.726	0.682	3.62
	400	0.738(22)	0.552(20)	1.104	0.819	3.62
	422	0.888(36)	0.430(37)	1.122	0.783	2.66
	511	0.988(14)	0.346(19)	1.138	0.767	2.66
	440	0.912(10)	0.463(12)	1.171	0.822	2.66

* Number(s) in the parentheses denote the standard uncertainty (s.u.) of the least significant digit(s). Only s.u.'s of refinable parameters are given.

TABLE III

Parameters obtained by diffraction line broadening analysis for samples S_1 and S_3: volume-weighted, $\langle D\rangle_v$, and surface-weighted, $\langle D\rangle_s$ domain sizes, root-mean-square strain averaged over a distance L in domains $\langle \varepsilon^2(L)\rangle^{1/2}$

Sample	$\langle D\rangle_v$ / nm	$\langle D\rangle_s$ / nm	$\langle \varepsilon^2(\langle D\rangle_v / 2)\rangle^{1/2} \cdot 10^3$
S_1	286(7)*	265(7)	0.23(1)
S_3	9.5(3)	5.9(2)	2.1(5)

* Number in the parenthesis denotes the standard uncertainty of the least significant digit.

analysis of line broadening is presented in Table III. Although the strain is 10 times larger for sample S_3 than for S_1, it still has a negligible influence on the broadening in comparison with the size effect. For instance, an estimate of strain by using the Stokes and Wilson[24] relation

$$e = \frac{\beta(2\theta)\cot\theta_0}{4} \tag{2}$$

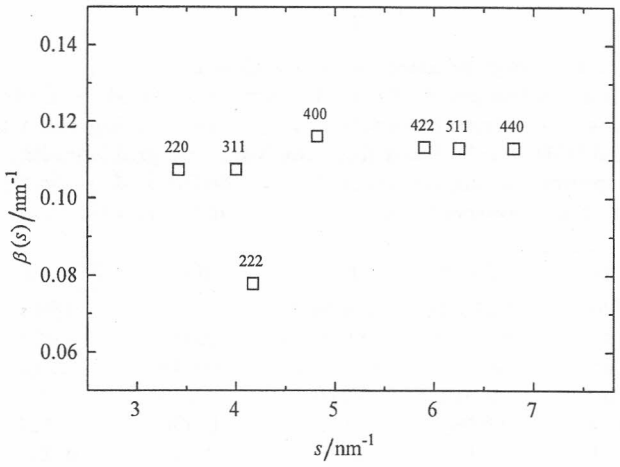

Figure 3. Williamson-Hall plot for sample S_3.

would require a strain of 0.012 to cause a line broadening comparable to the data from Figure 2 (we took $\beta(2\theta) = 1°$ at 40° 2θ). This is underlined by the fact that the value of volume-weighted domain size is reasonably close to the estimation from the Scherrer equation. It must be emphasized that the thus obtained domain size is an either volume-weighted or surface-weighted average thickness measured in the direction of the diffraction vector (orthogonal to the diffracting planes). Therefore, the real domain dimension will depend on its shape. In this particular case, it is safe to assume some isotropic shape. For instance, for a distribution of uniform spheres of diameter D it follows that $D = 4 \langle D \rangle_v / 3$, which gives the approximate average true domain dimension of 12.7(4) nm. This method goes beyond determination of a mere average value of domain size. It allows for the calculation of the domain-size distribution function. Figure 4 shows volume-weighted domain-size distribution functions for both S_1 (Figure 4a) and S_3 (Figure 4b) samples. The largest domain size for sample S_1 estimates to about 600 nm, whereas only 30 nm for S_3.

In conclusion, it is evident that the heating temperature, but not the heating time, has the ultimate effect on the particle size. Sample S_1, heated up to 1350 °C, shows a minimum diffraction-line broadening. It indicates well-defined and large crystallites without many crystal defects or site disorders.

Figure 5 shows characteristics parts of the FT-IR spectra recorded for samples S_1, S_2, S_4 and S_6. FT-IR spectrum of $NiFe_2O_4$ (sample S_1) is characterized by two bands with transmittance minima at 592 and 400 cm^{-1} and shoulders at 534, 468 and 342 cm^{-1}. The FT-IR spectra of samples S_2 to S_6 are characterized by the bands at 603 and 406 cm^{-1}. The shape of FT-IR

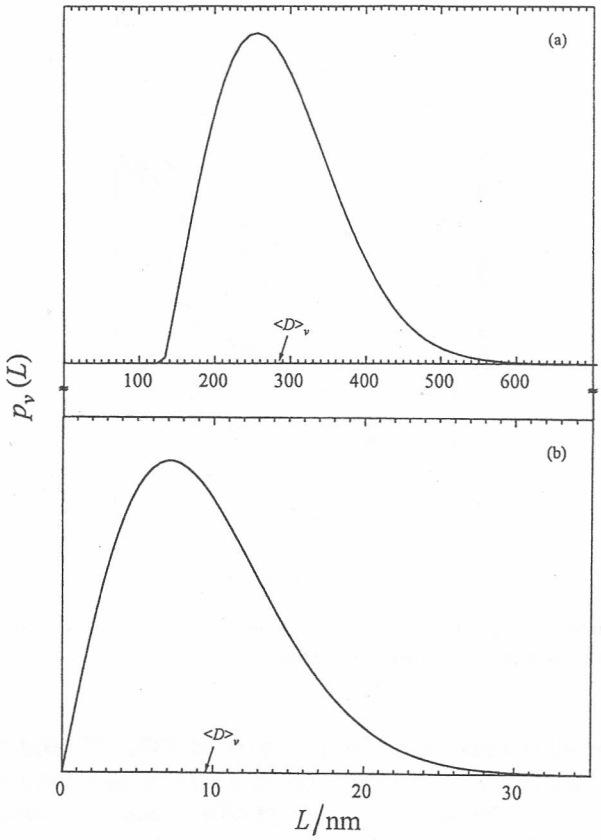

Figure 4. Volume-weighted domain-size distribution function normalized to the unit area. The average volume-weighted domain size is defined as a mean of this distribution: (a) sample S_1; (b) sample S_3.

spectra of samples S_7 and S_8 was similar to that of sample S_1 confirming the XRD results obtained for samples S_1, S_7 and S_8. Samples S_9 and S_{10}, prepared by heating the mixture of NiO : α-Fe_2O_3 = 1 up to 300 and 400 °C, respectively, did not show formation of nickel ferrite. When the temperature of heating was increased up to 800 °C, $NiFe_2O_4$ and ≈ 5% of α-Fe_2O_3 were found as the products of the solid state reaction (sample S_{11}).

The appearance of two very strong IR bands, at ≈ 600 and ≈ 400 cm^{-1}, is typical of the inverse spinel $NiFe_2O_4$.[6,25] In previous work,[7] it was observed that the IR bands of nickel ferrite shifted from 600 to 604 cm^{-1} and from 417 cm^{-1} to ≈ 400 cm^{-1} when the maximum temperature of heating changed from 700 to 1350 °C. The observed IR shifts were discussed in terms of crystal lattice ordering and/or change in stoichiometry of nickel ferrite. The shoulder at 529–536 cm^{-1} was pronounced best for nickel ferrite

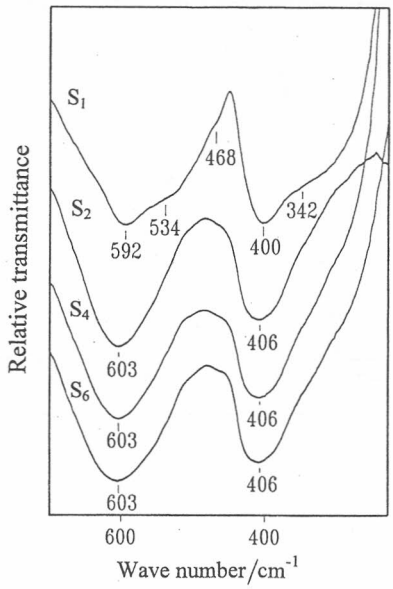

Figure 5. Characteristic parts of the FT-IR spectra of samples S_1, S_2, S_4 and S_6. The spectra were recorded at room temperature.

samples prepared at maximum temperature of 1350 °C, and this effect was not dependent on the preparation procedure such as chemical coprecipitation, solid state reaction between corresponding oxides or thermal decomposition of the mixed salts $Ni(NO_3)_2/Fe(NO_3)_3 \cdot nH_2O$. Incorporation of Cu^{2+} ions in $NiFe_2O_4$ caused a shift of IR bands at 608 and 417 cm^{-1} to smaller wave numbers and this was explained by the effect of Cu^{2+} (the Jahn-Teller ion) on the crystal field state of the Ni^{2+} ions.[26] The related Raman spectrum of $NiFe_2O_4$ was discussed by Graves *et al.*[27]

The present work indicates that $NiFe_2O_4$ as a single phase could be prepared by a simple thermal treatment of $Ni(OH)_2$ and $Fe(OH)_3$ without ceramic sintering. This means that distribution of Ni^{2+} and Fe^{3+} ions in the mixed hydroxide particles favours the formation of $NiFe_2O_4$, *i.e.*, that there are no preconcentration regions of Ni^{2+} or Fe^{3+} ions. Very probably, this could be related to the formation of $NiFe_2O_4$ precursor already during the precipitation of mixed hydroxide $Ni(OH)_2/Fe(OH)_3$ or in the early stage of its ageing.

The effect of mechanical treatment of $NiFe_2O_4$ on its structural properties was investigated by Pavlyukhin *et al.*[28] They observed a very strong effect on the Mössbauer spectrum. After 10 minutes of mechanical treatment of $NiFe_2O_4$, an intensive central doublet was observed at room temperature, while a symmetric central doublet was only present in the room temperature

spectrum after 30 minutes of mechanical treatment. The authors concluded that the observed effect is a consequence of the transfer of cations from the tetrahedral to vacant octahedral sites in the spinel structure. They also suggested that the disordering of anion and cation sites may lead to an X-ray amorphous structure.[28]

In contrast to the work by Pavlyukhin *et al.*,[28] such a dramatic influence of mechanical treatment on the properties of $NiFe_2O_4$ was not observed in the present work. Figure 6 shows Mössbauer spectra of $NiFe_2O_4$ before and after ball-milling for 27 hours at room temperature. No central quadruple doublet was observed. However, the calculated Mössbauer parameters (Table IV) indicated a decrease of hyperfine magnetic fields M_1 from 495 to 485 and M_2 from 526 to 516 kOe, during a ball-milling period up to 27 hours. The parameters of sextet M1 correspond to Fe^{3+} cations in tetrahedral sites, while the parameters of sextet M_2 correspond to Fe^{3+} cations in octahedral sites in $NiFe_2O_4$. The mechanical treatment of $NiFe_2O_4$ also caused an increase of the spectral line width and a slight increase of isomer shifts, as shown in Table IV. The FT-IR spectra (Figure 7) of the samples, obtained after ball-milling of $NiFe_2O_4$ did not show a significant change with the ball-milling time. A small change in the intensities of the shoulders at 534 and 332 cm^{-1} was visible. On the basis of Mössbauer and FT-IR measurements,

TABLE IV

^{57}Fe Mössbauer parameters of $NiFe_2O_4$ before and after ball-milling of different duration

Ball-milling time / h	Spectral component	Isomer shift* δ / mm s^{-1}	Quadrupole splitting ΔEq / mm s^{-1}	Hyperfine magnetic field H / kOe	Line width Γ / mm s^{-1}
0	M_1	0.237	–0.002	495	0.480
	M_2	0.352	–0.001	526	0.440
3	M_1	0.240	–0.002	495	0.525
	M_2	0.353	–0.002	527	0.461
6	M_1	0.238	–0.001	495	0.491
	M_2	0.350	–0.001	527	0.437
9	M_1	0.257	0.021	487	0.531
	M_2	0.356	0.010	517	0.449
15	M_1	0.269	0.010	486	0.506
	M_2	0.367	0.002	516	0.463
21	M_1	0.265	0.008	484	0.547
	M_2	0.366	–0.002	515	0.471
27	M_1	0.270	0.011	486	0.529
	M_2	0.368	–0.001	516	0.468

* Relative to α-Fe.

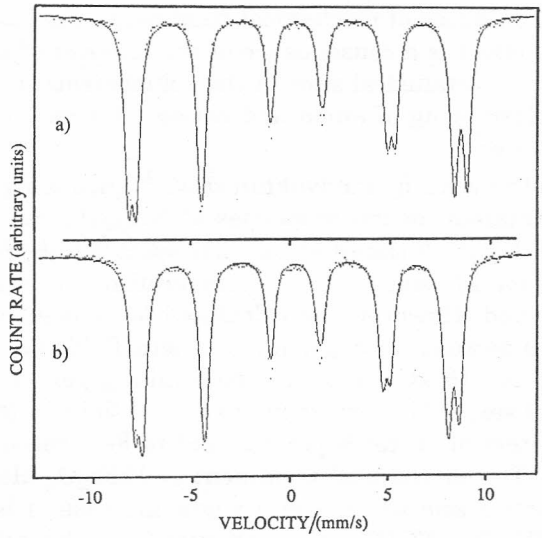

Figure 6. Mössbauer spectra (RT) of nickel ferrite (a) before and (b) after its ball-milling for 27 hours.

no conclusion can be drawn on the formation of an amorphous-like phase as a consequence of the ball-milling of $NiFe_2O_4$ under given experimental

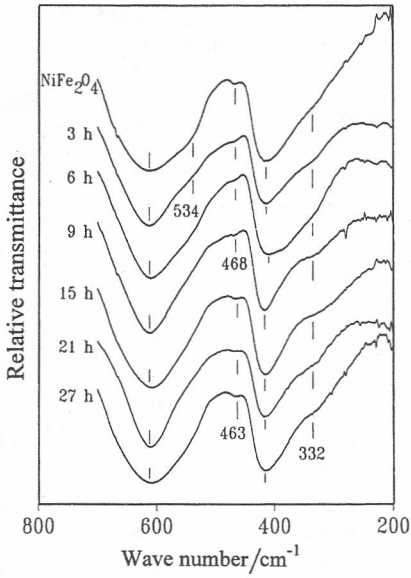

Figure 7. FT-IR spectra of nickel ferrite before and after ball-milling of different duration.

conditions. It can be supposed that the ball-milling of $NiFe_2O_4$ has a greater influence on the degree of inversion than on other structural properties of this spinel. However, we must keep in mind that Ni^{2+} has high preference for octahedral sites, as compared to Fe^{3+}. For this reason applied-field Mössbauer spectroscopic measurements must be performed, in the future to allow a more appropriate conclusion about the effect of ball-milling on the $NiFe_2O_4$ structure. The effect of mechanical grinding on the structural and magnetic properties of $BaFe_{12}O_{19}$ was also monitored by Mössbauer spectroscopy.[29–33] However, the mechanism of mechanochemical changes in M-type hexagonal ferrite is different than in the spinel ferrite $NiFe_2O_4$, due to the specific structure of $BaFe_{12}O_{19}$.[34]

Acknowledgements. – The authors gratefully acknowledge the support of (a) International Atomic Energy Agency (contract No 7681/RB), (b) National Research Foundation of Hungary (contract No TOO 7266) and (c) The USA (National Institute of Standards and Technology) – Croatia (Ministry of Science and Technology) Joint Fund (grant No JF106).

REFERENCES

1. V. Jha and A. K. Banthia, *Indian J. Phys.* **63A** (1989) 514–525.
2. A. H. Morrish and K. Haneda, *J. Appl. Phys.* **52** (1981) 2496–2498.
3. A. H. Morrish and K. Haneda, *J. Magn. Magn. Mater.* **35** (1983) 105–113.
4. V. Sitakara Rao, S. Rajendran, and H. S. Maiti, *J. Mater Sci.* **19** (1984) 3593–3601.
5. T. Morozumi, T. Fujii, T. Kozaki, and H. Ohashi, *Bull. Fac. Eng.* Hokkaido Univ., No. 141, 1988, p. 183–191.
6. S. Musić, S. Popović, and S. Dalipi, *J. Mater. Sci.* **28** (1993) 1793–1798.
7. S. Musić, S. Popović, I. Czakó-Nagy, and S. Dalipi, *Croat. Chem. Acta* **67** (1994) 337–346.
8. T. M. Peev, L. Bozadjiev, T. Stoilova, and S. Nikolov, *J. Radioanal. Nucl. Chem. Letters* **85** (1984) 151–162.
9. J. W. Linnett and M. M. Rahman, *J. Phys. Chem. Solids* **33** (1972) 1465–1473.
10. K. J. D. MacKenzie and C. M. Cardile, *Thermochim. Acta* **165** (1990) 207–222.
11. A. M. Gadalla and H.-F. Yu, *J. Mater. Res.* **5** (1990) 2923–2923.
12. Y. L. Sandler, *Corrosion* (NACE) **35** (1979) 205; cited in accordance with reference 13.
13. G. Raw, *The Synthesis and Characterisation of Magnetites and Nickel Ferrites,* Report-R10777, HARWELL, United Kingdom Atomic Energy Authority, April 1983.
14. D. A. Channing. M. J. Graham, and G. A. Swallow, *J. Mater. Sci.* **12** (1977) 2475–2487.
15. M. Lenglet, R. Guillamet, J. Lopitaux, and B. Hannoyer, *Mater. Res. Bull.* **25** (1990) 575–583.
16. S. Nagy and T. W. Weir, The Sirius Evaluating Program (The Mannual for Internal Use), Sinclair Laboratory, Lehigh University, Bethlehem. Pennsylvania, 1980.
17. H. P. Klug and L. E. Alexander, *X-ray Diffraction Procedures,* 2nd edition, John Wiley, New York, 1974, p. 661.
18. B. E. Warren, *X-ray Diffraction*, Dover Publications, New York, 1990, p. 251.
19. P. Scherrer, *Nachr. Gött.* **2** (1918) 98–100.

20. A. R. Stokes, *Proc. Phys. Soc. Lond.* **61** (1948) 382–391.
21. D. Balzar, *J. Appl. Crystallogr.* **25** (1992) 559–570.
22. D. Balzar and H. Ledbetter, *J. Appl. Crystallogr.* **26** (1993) 97–103.
23. G. K. Williamson and W. H. Hall, *Acta Met.* **1** (1953) 22–31.
24. A. R. Stokes and A. J. C. Wilson, *Proc. Phys. Soc. Lond.* **56** (1944) 174–181.
25. W. B. White and B. A. DeAngelis, *Spectrochim. Acta* **23A** (1967) 985–995.
26. C. M. Srivastava and T. T. Srinivasan, *J. Appl. Phys.* **53** (1982) 8148–8150.
27. P. R. Graves, C. Johnston, and J. J. Campaniello, *Mat. Res. Bull.* **23** (1988) 1651–1660.
28. Yu.T. Pavlyukhin, Ya.Ya. Medikov, and V. V. Boldyrev, *J. Solid State Chem.* **53** (1984) 155–160.
29. S. I. Campbell, E. Wu., W. A. Kaczmarek, and K. D. Iayasuriya, *Hyp. Interact.* **92** (1994) 933–941.
30. S. I. Campbell, W. A. Kaczmarek, E. Wu, and K. D. Iayasuriya, *IEEE Trans. Magn.* **30** (1994) 742–745.
31. W. A. Kaczmarek and Z. L. LI, *J. Mater. Sci.* **31** (1996) 491–498.
32. W. A. Kaczmarek and B.W. Ninham, *Mater. Chem. Phys.*. **40** (1995) 21–29.
33. V. A. Barinov, V. A. Tsurin, V. S. Gaviko, Ye. A. Yermakov, Ye. I. Teytel, N. I. Shegoleva, F. Leccabue, B. E. Watts, R. Panizzieri, G. Bocelli, and S. Diaz Castanon, *J. Magn. Magn. Mater.* **139** (1995) 143–150.
34. S. Musić, in: N. P. Cheremisinoff (Ed.), *Handbook of Ceramics and Composites,* M. Dekker Inc., New York 1992, pp. 423–463.

SAŽETAK

Nastanak i svojstva $NiFe_2O_4$

Svetozar Musić, Davor Balzar, Stanko Popović, Marijan Gotić, Ilona Czakó-Nagy i Samet Dalipi

$NiFe_2O_4$ je pripravljen grijanjem mješovitoga metalnog hidroksida odgovarajućeg sastava ili reakcijom NiO i α-Fe_2O_3 u čvrstom stanju. Pripravljeni uzorci istraživani su rentgenskom difrakcijom, FT-IR spektroskopijom i ^{57}Fe Mössbauerovom spektroskopijom. Intenzivno mljevenje $NiFe_2O_4$ uvjetovalo je smanjenje hiperfinoga magnetskog polja iona Fe^{3+} u tetraedarskim i oktaedarskim položajima, povećanje širine Mössbauerovih spektralnih linija i malo povećanje izomernih pomaka. Zaključeno je da mljevenje $NiFe_2O_4$ ima više utjecaja na stupanj inverzije $NiFe_2O_4$ nego na ostala svojstva tog spinela. Utvrđeno je da temperatura grijanja, a ne vrijeme grijanja, ima odlučujuće djelovanje na mikrostrukturu $NiFe_2O_4$. Uzorci grijani do 500 °C pokazali su izrazito širenje rentgenskih difrakcijskih linija, uzrokovano veličinom kristalita od približno 13 nm i relativno malom kristalnom neuređenošću. Uzorci grijani iznad ≈ 1000 °C posjedovali su puno veće kristale koji su pokazivali vrlo malu kristalnu neuređenost.